This full text paper was peer reviewed at the direction of IEEE Communications Society subject matter experts for publication in the IEEE Secon 2010 proceedings.

N-Body: Social Based Mobility Model for Wireless Ad Hoc Network Research

Chen Zhao and Mihail L. Sichitiu
Department of Electrical and Computer Engineering
North Carolina State University
Raleigh, NC 27606
Email: czhao4@ncsu.edu, mlsichit@ncsu.edu

***Abstract*—Accurate reproduction of real human movement patterns is necessary in simulations of mobile ad hoc networks in order to obtain meaningful performance results. Human activities are often socially organized, resulting in a certain level of tendency of forming groups. There exists a few mobility models that are taking this tendency into account; however, all these models require a certain level of understanding of the underlying social structure of the target scenario, which limits their application scope. In this paper we propose an N-body mobility model that tackles such social aspects from a different perspective. We extract the social information from real human movement traces, and reproduce them in the mobility model. We show that the N-body model is capable of capturing and synthesizing the group-forming tendency that matches to those observed from sample traces. Simulation results also show that N-Body models exhibit a similar pairwise heterogeneity in ad-hoc network performance as the sample traces do.**

I. Introduction

Research on mobile ad hoc networks (MANETs) or delay tolerant networks (DTNs) is still heavily based on simulation due to the lack of real deployments. To accurately evaluate the performance of such networks, the mobility models that generate nodal movements during simulations are of crucial importance [1]. Most models assumes that all nodes move independently without any inter-nodal correlation, e.g., the widely implemented random walk (RW) and random waypoint (RWP) [2]. In real life, however, people are often related with each other through a complex *social network*, which is known to be highly clustered [3] as well as showing small world effects [4], [5]. Such social nature also affects human mobility: on many occasions people tend to move in groups, rather than individually. e.g., students attending lectures, platoons moving on the battlefield, families walking around at the state fair, or rescue squads searching for victims. On the other hand, such groups may be dynamic and of different strengths. People may stay in different groups at different times or even linger among several groups at the same time. Some groups may be tight and have fixed members, while others are loose and temporary. Therefore, real human movements can be quite heterogeneous. In recent works [6], [7] such complex heterogeneity is well observed in mobility traces and is shown to affect the performance of both MANETs and DTNs.

Several mobility models aware of such heterogeneity have been proposed in recent years [8]–[24]. The Reference Point Group Model (RPGM) [8] is perhaps the earliest work taking such grouping tendency into account. In RPGM nodes are divided into groups and move randomly around the group centers, which are also moving. It is a direct and intuitive way to synthesize such tendency. Several variances of RPGM were proposed later in [9]–[14] with refined patterns of group-wise movements [9], [10] or intra-group movements [10]–[13], or with fine-grained structures inside groups [14]. However, all these models require explicit division of the population into groups, which do not represent situations where inter-personal relationships are complex.

Another class of models [15]–[19] was proposed with the dynamics similar to early preferential attachment models in [25], [26]. These models require an $N \times N$ numerical matrix (often referred to as the social matrix) for an N node system, with each entry representing the strength of the social bond between the two corresponding nodes. The model in [15] derives a fixed meeting schedule for each node according to the cliques in the social matrix, and the strength of relationship corresponds to the frequency and duration of meetings. In models proposed in [16], [17], the selection of nodes' destinations is influenced by their friends, with the social matrix corresponding to the influence level. In addition, the model in [17] also incorporates flock behavior studied in [27]. The model in [18] behaves similar to RPGM, but determines the pause time based on the nodes' relationship with its neighbors. In [19] nodes are attracted to their friends, and they repulse each other once they've been together for long enough. All these models provide means to incorporate a numerical social matrix into the model dynamics. However, the derivation of such matrices requires an in-depth understanding of both the simulation scenario and the model dynamics, which is non-trivial due to the complex interaction between the underlying social structure and the model dynamics. Therefore these models all have limited application scope.

A third class of models tackles the network heterogeneity as a result of geographical heterogeneity between individual nodes [20], [21]. Although these models do produce spatially correlated movements, such movements are not essentially group movements in terms of stationarity. Yet another class of models proposed in [22]–[24] implement detailed role models to produce group movements. These models share the same shortcomings of those numerical matrix based models regarding the limited application scope.

978-1-4244-7151-5/10/$26.00 ©2010 IEEE

In this research, aware of the shortcomings of existing models, we propose the *N-Body Mobility Model* inspired by n-body simulations [28]. As shown in in Fig. 1, **rather than getting into the details of the social scenario, we simply capture some social metrics from an input trace and synthesize them in the N-Body model.** The output trace is validated against the input trace. Thus, the N-Body model is designed to reproduce the heterogeneity of the input trace. In particular, we implemented mutual forces between nodes in the model dynamics to achieve such heterogeneity.

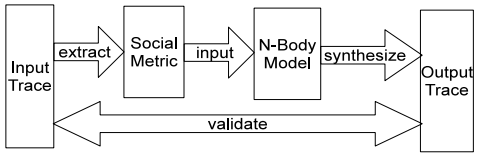

Fig. 1. Block diagram of N-Body model framework.

Using forces or similar means to adjust nodal movements has been considered in several previous works [11]–[13], [17]. In an early work [11] the authors implemented speed adjustments in an ad hoc manner to mimic the flock behavior studied in [27]. Later similar dynamics were also implemented in [12], [17]. In [13] the authors used attraction and repulsion forces to mimic the flock behavior and provide obstacle avoidance. However, all these previous works used such dynamics only as a means of movement smoothing and collision avoidance on a fine level, rather than coordinating nodes to produce correlated movements. To synthesize correlated movements these models either explicitly divide the population into groups [12], [13], or correlate the nodes' destination selection [17], or use pre-defined movement patterns [11]. The N-Body model differs from earlier works in that all correlated movements are completely and quantitatively controlled by inter-nodal forces.

Compared with previous models, the advantage of our model is three-fold:

- First, it doesn't require detailed knowledge of the target scenario; therefore it has wider application scope.
- Second, since numeric social metrics are used as input of our model, the extent of such heterogeneity can be quantitatively controlled and studied.
- Finally, the dynamics based on Gay-Berne potential mimics the speed matching, group centering and collision avoidance behavior of flock movements [27], thus the nodal movements are realistic on the fine level.

The rest of this paper is organized as follows: Section II quantifies the social aspects by observing real movement traces and uses them as the measure of group-forming tendency. Section III describes the detailed settings and dynamics of the N-Body model. Section IV validates the N-Body model by comparing the performance of our model with the original trace through simulation. Section V summarizes our contribution and proposes the future work.

II. Social Metrics

To synthesize mobility traces that show the heterogeneity of the input trace, the nodes' group-forming tendencies need to be quantified as the social metrics in Fig. 1. When nodes are moving in groups, their relationship is reflected in the statistics of the pairwise inter-nodal distances among the group members.

A. Friendship / Steadiness Matrices

In the following scenario we assume a total of N nodes $n_i,\ i = 1, ..., N$, moving in the vector space $\mathbf{\Omega}$ with their positions at time t being $\vec{P}_i(t) \in \mathbf{\Omega}$. The pairwise distance between two arbitrary nodes n_i and n_j is the following random process:

$$D_{i,j}(t) = \left| \vec{P}_i(t) - \vec{P}_j(t) \right|, \tag{1}$$

whose mean $M_{i,j}$ and *normalized* standard deviation (NSD) $S_{i,j}$ can be estimated from the recorded traces, which is assumed to consist of the nodes' locations sampled at consecutive time points, e.g., a total of L time points $t_l = l\Delta t,\ l = 1, 2, \ldots L$ with an equal interval Δt. Assuming the nodal movements are stationary, the mean and NSD can be estimated:

$$M_{i,j} \approx \widetilde{M}^L_{i,j} = \frac{1}{L} \sum_{l=1}^{L} \left| \vec{P}_i(t_l) - \vec{P}_j(t_l) \right|, \tag{2}$$

$$S_{i,j} \approx \widetilde{S}^L_{i,j} = \sqrt{\frac{\sum_{k=1}^{L} \left| \vec{P}_i(t_l) - \vec{P}_j(t_l) \right|^2}{(L-1)\widetilde{M}^{L}_{i,j}{}^2} - \frac{L}{L-1}}. \tag{3}$$

To capture the group-forming tendency, we compare $M_{i,j}$ and $S_{i,j}$ with those of *independent random placement* (IRP), which is the distance between nodes when they are independently placed according to the stationary nodal distribution. The corresponding mean and NSD is denoted by M^{IRP} and S^{IRP}:

$$M^{\mathrm{IRP}} = \iint_{\mathbf{\Omega}^2} \left| \vec{P} - \vec{P}' \right| \lambda(\vec{P}) \lambda(\vec{P}') \mathrm{d}\vec{P} \mathrm{d}\vec{P}', \tag{4}$$

$$S^{\mathrm{IRP}} = \sqrt{\frac{\iint_{\mathbf{\Omega}^2} \left| \vec{P} - \vec{P}' \right|^2 \lambda(\vec{P}) \lambda(\vec{P}') \mathrm{d}\vec{P} \mathrm{d}\vec{P}'}{M^{\mathrm{IRP}\,2}} - 1}, \tag{5}$$

where $\vec{P}$ and $\vec{P}'$ are two independent random vectors following the stationary nodal distribution λ. By comparing with $M_{i,j}$ and $S_{i,j}$, we define the *friendship index* $r_{i,j}$:

$$r_{i,j} = 1 - \frac{M_{i,j}}{M^{\mathrm{IRP}}},\ r_{i,j} \in (-\infty, 1], \tag{6}$$

and the *steadiness index* $w_{i,j}$:

$$w_{i,j} = \frac{S_{i,j}}{S^{\mathrm{IRP}}},\ w_{i,j} \in [0, \infty). \tag{7}$$

By inspecting the indices $r_{i,j}$ and $w_{i,j}$ the static and dynamic aspects of the pairwise group-forming tendency can be revealed. When $r_{i,j} > 0$, the two nodes n_i and n_j are closer to each other than one would expect from two independent (IRP) nodes; thus they show a positive tendency of moving in a group. When $r_{i,j} < 0$, the negative tendency could be interpreted as the two nodes are trying to stay away from each other. On the other

hand, the NSD reflects the steadiness of the group; e.g., node pairs with $w_{i,j} < 1$ are likely to stick to their positions inside the group rather than wander around, and vice versa. Since $r_{i,j}$ captures the group structure, it is regarded as the *primary index* during later synthesis while $w_{i,j}$ is the *secondary index*.

Since both the pairwise mean distance $M_{i,j}$ and that of IRP M^{IRP} assume the same stationary nodal distribution, **simple population hotspots, e.g., airports or shopping centers in a city, do not affect** $r_{i,j}$; while traffic restrictions that affect movement patterns do, e.g., when nodes are moving on the highway adjacent nodes form temporary groups. It is shown in Section IV-B when comparing performance results between the original traces, the N-Body models and improved RWP with empirical hotspots, that simply implementing hotspots does not account for the pairwise heterogeneity.

For an N node system, all the indices comprise the $N \times N$ *friendship matrix* and *steadiness matrix*:

$$R = \begin{bmatrix} r_{1,1} & \dots & r_{1,N} \\ \vdots & \ddots & \vdots \\ r_{N,1} & \dots & r_{N,N} \end{bmatrix}, W = \begin{bmatrix} w_{1,1} & \dots & w_{1,N} \\ \vdots & \ddots & \vdots \\ w_{N,1} & \dots & w_{N,N} \end{bmatrix}. \tag{8}$$

Both are symmetric with the diagonal elements undefined.

B. Sample Traces

We extracted these indices from RWP and RPGM as well as two real-life traces: the bus trace in Seattle from Ad-Hoc City project [29] and taxicab trace in San Francisco from Cabspotting project [30]. For all traces, we consider 48-50 nodes running for 16 hours. The sample interval is 4 seconds and the two real traces are linearly interpolated.

The Seattle bus trace (STBUS) contains GPS logs of more than 1200 buses running 239 routes for about 20 days. Bus locations are updated every 2 minutes. Since there are frequent holes in the trace, we extracted *flights* out of the trace, which are continuous records of a bus running one route. We chose 48 longest flights running 7 routes for at least 16 hours, and time-shifted them so they start at the same time. Thus, such a trace will show higher group-forming tendency between buses running the same routes.

The SF cab trace (SFCAB) contains GPS logs of 536 cabs for over 30 days. Records are updated every minute if the cab is online. We selected 50 cabs that stayed online together for at least 16 hours. Most the cabs should move independently, however, due to the geographical restraints (like highways), there may exist some modest level of group-forming tendencies.

Both the RWP and RPGM models are set on a $20 \times 20\mathrm{km}$ plane which resembles the dimensions of a downtown like Seattle or SF. RWP has 50 nodes with uniform speeds from 3 to $12\mathrm{m/s}$, which are typical city speeds. RPGM has 48 nodes in 4 groups with 12 nodes each. Two groups have a radius of $500\mathrm{m}$ while the other two have $2\mathrm{km}$. Groups move at $5\mathrm{m/s}$ and nodes randomly drift within the groups' radius also at $5\mathrm{m/s}$. No pause was implemented for both models.

We plotted the cumulative distribution functions (CDF) of the pairwise friendship index $r_{i,j}$ in Fig. 2. As expected, RWP has its friendship indices concentrated around 0, indicating homogeneous pairwise relationships without any group-forming tendency. For RPGM, from the upper right steps it is clear that nodes from the same groups show different levels of group-forming tendency, which is caused by different group radius. Nodes from different groups, however, have their $r_{i,j}$ concentrated around 0 just like in RWP. The SFCAB trace is similar to RWP, but with an increased level of heterogeneity as well as higher group-forming tendency because of the geographical restrictions as mentioned above. The STBUS trace shows an even higher level of heterogeneity. To better understand this trace, we separated its $r_{i,j}$ data into those running the same routes and those running different routes, and plotted their CDFs in the inset. Compared to the buses running different routes, those running the same routes have much higher group-forming tendencies, although there are some pairs showing negative tendencies, which is caused by imperfect trace processing as some flights are not correctly aligned in time.

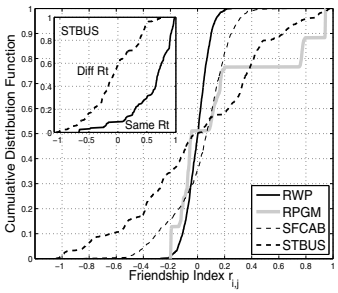

Fig. 2. CDF of pairwise friendship index r_{ij} for all 4 traces. Inset: for flights from the same / different routes in the STBUS trace.

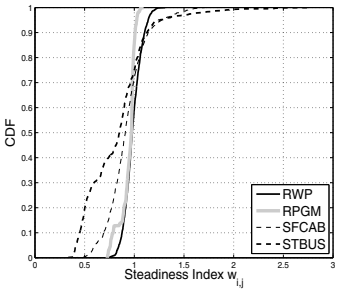

Fig. 3. CDF of pairwise steadiness index w_{ij} for all 4 traces.

Similar to the friendship index, we also plotted the CDFs of the pairwise steadiness index $w_{i,j}$ in Fig. 3. It is shown that RWP has its steadiness indices converging towards 1, which is to be expected from a homogeneous model. RPGM has similar distribution to RWP, due to its similar dynamics with that of RWP for both nodes from different groups and nodes from the same groups, regardless of the group radius. Both SFCAB and STBUS traces have the steadiness indexes $w_{i,j}$ spanning a wider range, which indicates higher diversity in their NSD than RWP or RPGM.

III. N-Body Mobility Model

In this section we propose the N-Body mobility model, which as shown in Fig. 1, uses the social metrics extracted from input traces in Section II as its input, and synthesize traces that show similar heterogeneity that matches the input metrics.

A. Basic Dynamics

The dynamics of N-Body model are based on that of RWP [2] (may incorporate empirical results into parameters like speed, pause or even hotspots as in [31]–[33]) but with movements driven by attraction forces towards destinations as well as mutual forces between nodes. By implementing such multi-body interaction, which is often seen in the dynamics of n-body movements [28], users can fine-tune the group-forming tendencies between nodes towards the desired targets.

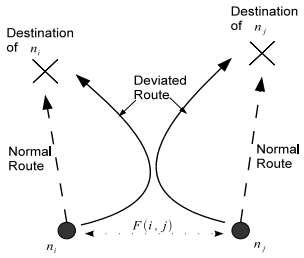

Fig. 4. Two nodes n_i and n_j with a strong grouping tendency are attracted to each other by the inter-nodal force $F_{i,j}$, thus deviating from their normal route and move together for a while, like two friends talking to each other for a while on their way to work.

At the start of the simulation, all nodes randomly select their destinations like in RWP (or according to empirical popularity as in [31]–[33]). Afterwards the nodes are attracted towards their destinations. They also interact (via forces) with other nodes such that their actual trajectories may deviate from their normal straight routes as shown in Fig. 4. Once the nodes reached the destinations they pause for some time and move on to their next destinations.

Since nodal movements are force driven, the N-Body model is implemented as a time stepping simulator using the improved Euler's method [34] with step time Δt. The basic dynamics are described below:

1) At time $t = 0$ each node n_i is randomly placed at $\vec{P}_i$ in the simulation area and is marked as ready (nodes can be in one of the three states: ready, in-flight, in-pause).
2) Select the next destination (either randomly or based on empirical hotspots) for each node marked ready. Mark these nodes as in-flight.
3) Calculate the forces imposed on each node n_i marked in-flight:

$$\vec{F}_i = \vec{G}_i + \sum_{j \neq i} \vec{F}_{j,i} = g(\vec{P}_i, i = 1 \ldots N), \qquad (9)$$

where $\vec{G}_i$ is the attraction force from the destination, and $\vec{F}_{j,i}$ is the inter-nodal force from another node n_j. Update its position $\vec{P}_i$ and velocity $\vec{v}_i$ over this time step using the improved Euler's algorithm.
4) If any in-flight nodes have reached their destinations (or within some threshold distance), mark them as in-pause. Choose a pause time (either randomly or according to empirical distributions) for each node.
5) If any in-pause nodes have reached their pause time, mark them as ready.
6) Step the time forward $t = t + \Delta t$. Go to step 2.

B. Attraction and Speed Control

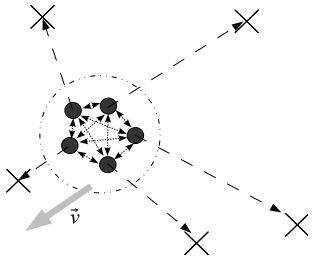

Fig. 5. Several nodes are attracted to each other and form a clog. They move as a whole and visit the destinations according to their distances.

For an arbitrary node n_i, we denote the attraction force from its destination as $\vec{G}_i$, and the mutual force from another node n_j as $\vec{F}_{j,i}$ ($\vec{F}_{j,i} = -\vec{F}_{i,j}$). If the two nodes have positive group-forming tendency, the mutual forces $\vec{F}_{j,i}$ and $\vec{F}_{i,j}$ will pull them together so that they will be closer to each other as shown in Fig. 4. When nodes have very strong mutual forces between them, they form a clog as shown in Fig. 5 and cannot be separated. Thus, the nodes will move together as a group as the attraction forces to the destinations competing with each other. To avoid tie-ups, the destination attraction forces are set to be inverse proportional to the distance between the nodes and their destinations:

$$\vec{G}_i = G_0 \frac{d_0}{\left|\vec{d}_i\right|} \hat{d}_i, \qquad (10)$$

where $\vec{d}_i$ is the distance vector from n_i towards its destination and $\hat{d}_i$ is the corresponding unit vector, G_0 is the unit force, and d_0 is a reference distance at which the attraction is G_0[1].

When nodes forms a clog and the attractions are competing against each other, the nearest destination will often win out, and the group will visit the destinations in the sequence according to their distances as shown in Fig. 5. Near-ties are easily broken since the balance is unstable: a small move in any direction will enhance the forces towards that direction while weakening the opposite ones. Once the group reaches a destination it may even pause as a whole if the mutual forces among the nodes are strong.

[1]The reference distance d_0 is set to the average IRP distance M^{IRP} from (4), therefore the nodes would on average receive an attraction of G_0.

To control speeds, each node is assigned a maximum speed v_{iM}. A node may accelerate, decelerate or change its direction due to attractions and mutual forces, but its speed never exceeds v_{iM}. When updating speeds during each time step, the speed is truncated to v_{iM}. Assignments of the speed limit may be flexible. Nodes may share the same limit, or each may have a different one, or even chooses one at the beginning of each flight as in RWP.

Hence, when there is no mutual force between nodes, after a period of acceleration, the node will be moving at its speed limit v_{iM} towards the destination. If G_0 is chosen sufficiently large so that the acceleration time is negligible, and no mutual force is considered, the N-Body model reduces to RWP.

C. Mutual Force

The mutual forces must be carefully determined since they play a central role in adjusting the pairwise nodal distances. In the pioneering paper [27] the author studied the animal flock motion and summarized the flock behavior as collision avoidance, velocity matching and flock centering, which were later synthesized in mobility models in [11], [13], [17]. In a recent paper [35] the author pointed out that such flock behaviors can be easily synthesized by implementing the Gay-Berne potential [36], which was used in modeling inter-molecular forces. Inspired by this conclusion, we implemented the mutual forces in the form of a simplified Gay-Berne potential:

$$\vec{F}_{j,i} = 4G_0\epsilon \left[\frac{s}{\left|\vec{d}_{i,j}\right| + s - \sigma} - \frac{s^2}{\left(\left|\vec{d}_{i,j}\right| + s - \sigma\right)^2} \right] \hat{d}_{i,j}, \tag{11}$$

where $\vec{d}_{i,j}$ denotes the distance vector from node n_i towards n_j, and parameters ϵ, s and σ shape the relationship between $|\vec{F}_{i,j}|$ and $|\vec{d}_{i,j}|$ as shown in Fig. 6.

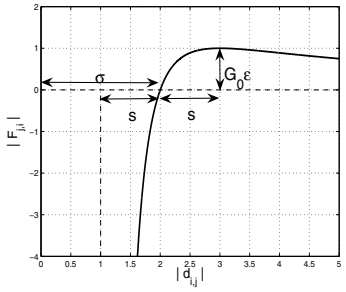

Fig. 6. Inter-nodal force as a function of distance ($\epsilon = 1$, $s = 1$, $\sigma = 2$).

Figure 6 shows the mutual force $\vec{F}_{j,i}$ as a function of the distance $|\vec{d}_{i,j}|$. When the two nodes are far from each other, i.e., $|\vec{d}_{i,j}| > \sigma$, there is a weak attraction force between them; as they get closer, the force becomes stronger, which implies that nodes are more attracted to friends nearby rather than those far away. The attraction force reaches its maximum of ϵG_0 when $|\vec{d}_{i,j}| = s + \sigma$. Afterwards it decreases, and is reduced to 0 when $|\vec{d}_{i,j}| = \sigma$. As the two nodes get even closer, the attraction turns to repulsion, and approaches infinity when the nodes get too close as $|\vec{d}_{i,j}| \to (\sigma - s)^+$ if $\sigma > s$.

Intuitively, the attraction forces between far away nodes pull them together so as to mimic velocity matching and flock centering, while the repulsion forces between closer nodes avoid collisions [27], [35]. While σ sets the optimal distance between two nodes, s indicates the maximum span of this attraction-repulsion force, thus they are directly related to the mean and NSD of the pairwise nodal distances. The parameter ϵ sets the strength of such force in influencing nodal movements. Therefore, to finely control the pairwise nodal distances such that they may approach the desired mean and NSD, a unique set of the parameters ϵ, s and σ are assigned to each pair of nodes. For convenience, we define the *interaction vector*:

$$\eta_{i,j} = (\epsilon_{i,j}, s_{i,j}, \sigma_{i,j}). \tag{12}$$

All such vectors in the system comprise an $N \times N$ matrix:

$$Q = \begin{bmatrix} \eta_{1,1} & \cdots & \eta_{1,N} \\ \vdots & \ddots & \vdots \\ \eta_{N,1} & \cdots & \eta_{N,N} \end{bmatrix}. \tag{13}$$

Q is referred to as the *interaction matrix*. It is symmetric with undefined diagonal elements.

D. Closed Loop Pre-Synthesis

To synthesize the desired pairwise nodal distances, when all other parameters of the N-Body model have been specified, the problem is reduced to finding the appropriate interaction matrix Q such that the actual friendship and steadiness matrices (denoted by R' and W') approximate the ones from the trace:

$$(R', W') = \mathscr{F}(Q) \approx (R, W), \tag{14}$$

where $\mathscr{F}$ denotes the N-Body process that produces the results R', W' with the input Q.

Ideally, it is straightforward to find a numeric solution for (14) if there is a one-to-one relationship between individual elements of R', W' and Q:

$$\left(r'_{i,j}, w'_{i,j}\right) = \mathscr{G}(\eta_{i,j}), \tag{15}$$

where $\mathscr{G}$, if exists, maps the individual interaction vector $\eta_{i,j}$ to the corresponding indices $(r'_{i,j}, w'_{i,j})$.

Unfortunately, (15) almost never holds. The distance between two nodes depends on interactions not only between themselves, but also with their friends, since increasing the attraction force between a pair of nodes would also shorten distances between their mutual friends. Thus, it is not feasible to obtain any direct solution of (14). A practical way to solve the problem is to use a *closed loop pre-synthesis* before the actual trace generation: start with a pre-specified Q, synthesize the trace for some period of time T_c, calculate the actual matrices R' and W' and adjust Q according to their difference to the target R and W, then repeat this epoch with the new Q until the results are sufficiently close to the target. In this way, despite of the complex interactions between nodes, an appropriate interaction matrix Q may be approximated on an individual pair basis, e.g.,

for each pair of nodes n_i and n_j, adjust only the corresponding $\eta_{i,j}$ accordingly during each cycle if there is a discrepancy between their actual and target pairwise nodal distance, namely, the mean $M_{i,j}$ and NSD $S_{i,j}$.

Thus, to effectively adjust $\eta_{i,j}$, we need to understand the influence of parameters $\epsilon_{i,j}$, $s_{i,j}$ and $\sigma_{i,j}$ on $M_{i,j}$ and $S_{i,j}$. Inferring from Fig. 6 and the discussion in Section III-C, we have the following conclusions (also summarized in Table I):

- Adjusting $s_{i,j}$ or $\sigma_{i,j}$ is effective only when $\epsilon_{i,j}$ is significantly large, i.e., when the resulting mutual force is comparable to the average gravity G_0.
- Increasing $\epsilon_{i,j}$ will push the two nodes towards $\sigma_{i,j}$ and restrain them from deviation. In fact, as $\epsilon_{i,j} \to \infty$, the two nodes will be "locked" with $M_{i,j} \to \sigma_{i,j}$ while $S_{i,j} \to 0$.
- $\sigma_{i,j}$ is directly proportional to the average distance $M_{i,j}$. In fact, $M_{i,j}$ is often at the close neighborhood of $\sigma_{i,j}$.
- Increasing $s_{i,j}$ increases the span of the inter-nodal force and therefore, releases the pair of nodes from being "locked" at the distance $\sigma_{i,j}$, thus will increase $S_{i,j}$.

TABLE I
INFLUENCE OF INDIVIDUAL PARAMETERS

Adjustment	$M_{i,j}$	$S_{i,j}$
$\epsilon_{i,j}$ ↗	Closer to $\sigma_{i,j}$	↘
$\epsilon_{i,j}$ ↘	Away from $\sigma_{i,j}$	↗
$\sigma_{i,j}$ ↗	↗	N/A
$\sigma_{i,j}$ ↘	↘	N/A
$s_{i,j}$ ↗	N/A	↗
$s_{i,j}$ ↘	N/A	↘

Before the pre-synthesis starts, the parameters are assigned the initial values: $\epsilon_{i,j} = G_0/(N-1)$, $\sigma_{i,j} = M_{i,j}$ and $s_{i,j} = S_{i,j} \cdot M_{i,j}$, where N is the total number of nodes. The parameter $\epsilon_{i,j}$ is assigned the above value so that the maximum total attraction upon each node is G_0. Afterwards, during the closed loop pre-synthesis, after comparing the actual and target mean and NSD, all the parameters are adjusted according to their impact as summarized in Table I until the actual metrics are sufficiently close to the targets.

IV. SIMULATION AND VALIDATION

We validate our model by comparing its performance with the input traces. The N-Body mobility model is currently implemented in Matlab.

A. Influence of Individual Parameters

Before synthesizing the traces for target scenarios, we first validate the influence of the individual parameters $\epsilon_{i,j}$, $s_{i,j}$ and $\sigma_{i,j}$ on the actual mean and NSD of the pairwise distances as discussed in Section III-C and III-D. We run an N-Body simulation with two nodes on a 200m × 200m plane with no hotspots or pause. The unit force (acceleration) is set to $G_0 = 1\text{m/s}^2$ with the reference distance $d_0 = 140$m, which is about the average IRP distance calculated from (4) using the stationary nodal distribution of RWP from [37]. Each node has the same maximum speed 5m/s. The simulator proceeds

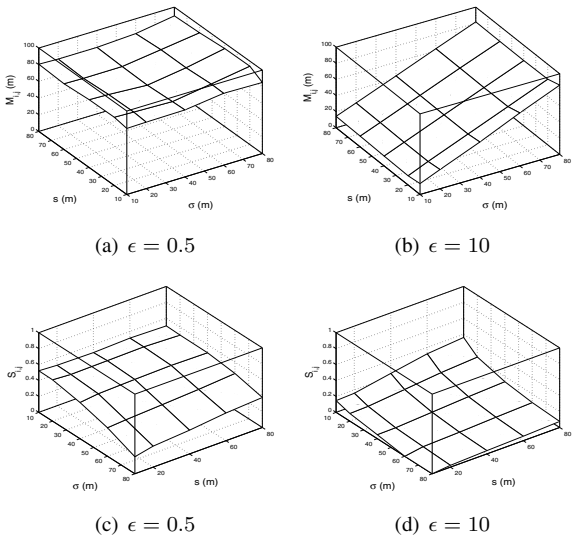

(a) $\epsilon = 0.5$ (b) $\epsilon = 10$

(c) $\epsilon = 0.5$ (d) $\epsilon = 10$

Fig. 7. Influence of individual parameters on the mean $M_{i,j}$ (a)(b) and NSD $S_{i,j}$ (c)(d) of the pairwise distances. Parameter: (a)(c) $\epsilon = 0.5$, (b)(d) $\epsilon = 10$. The σ axis is transposed in (c)(d) for improved visibility.

at time step $\Delta t = 1$s, and node locations are sampled every 8 seconds. Each simulation lasts 4 hours.

For each run we specify different ϵ, s and σ parameters. The resulting mean and NSD of their distances are shown against σ and s in Fig. 7 with $\epsilon = 0.5, 10\text{m/s}^2$, respectively. When ϵ is low ($\epsilon = 0.5$) as shown in Fig. 7(a) and 7(c), adjusting s and σ does not make a large difference. When ϵ is significantly high ($\epsilon = 10$), from Fig. 7(b) it is shown that the mean is mainly determined by σ, and from Fig. 7(d) the NSD is shown to be proportional to s with given σ. Increasing σ also decreases NSD since it increases the mean.

B. Synthesis from Input Traces

TABLE II
PARAMETERS FOR SIMULATING TARGET SCENARIOS

Parameters	RPGM	SFCAB	STBUS
Node Num	48	50	48
Area (km × km)	20 × 20	61 × 47	24 × 30
Ref Distance d_0 (m)	7287	4785	9184
Unit Force G_0 (m/s^2)	1		
Avg Speed (m/s)	6.5	6.3	4
Avg Pause (s)	0	56	297
Step Time T_{step} (s)	4		
Total Simulation Time (hour)	16		
Contact Range (m)	2500	2000	3000

To validate the N-Body model we synthesize traces showing social metrics similar to those extracted from the traces in Section II, namely, the RPGM, SFCAB and STBUS traces. The parameters are set according to the target scenarios as summarized in Table II. Assuming all nodes move with the same maximum speed and follow an exponential pause time distribution, the average speeds, pause times and total simulation times are extracted from the traces. Reference distances d_0 are set to the average IRP distance $M_{i,j}^{\text{IRP}}$ which are calculated from (4). For

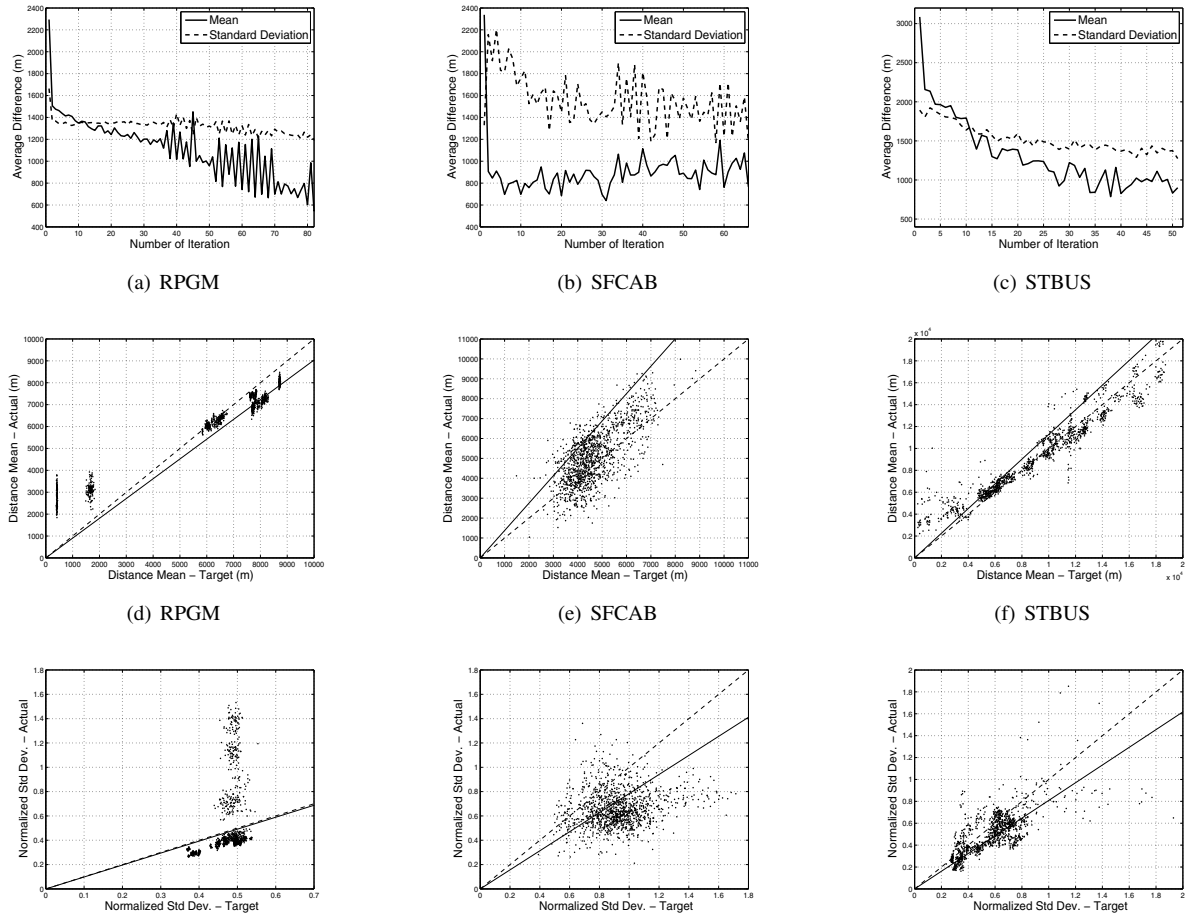

(a) RPGM (b) SFCAB (c) STBUS

(d) RPGM (e) SFCAB (f) STBUS

(g) RPGM (h) SFCAB (i) STBUS

Fig. 8. Trends of convergence during the closed loop pre-synthesis (a)(b)(c) and convergence results at the end of pre-synthesis as target versus the actual mean distance $M_{i,j}$ (d)(e)(f) and NSD $S_{i,j}$ (g)(h)(i). Mobility Models: (a)(d)(g) RPGM, (b)(e)(h) SFCAB, (c)(f)(i) STBUS. Solid lines in (d)-(i) have the slope of the ratio between $M^{\text{IRP}\prime}$ and M^{IRP} or between $S^{\text{IRP}\prime}$ and S^{IRP}. Dashed lines have the slope of 1.

better synthesis accuracy, hotspots are also implemented. The simulation area is divided into a total of K grids (1km $\times$ 1km grids for SFCAB and STBUS, 200m $\times$ 200m for RPGM), and a probability of selection μ_k $(k \in [1 \dots K], \sum \mu_k = 1)$ is calculated for each grid from the input traces as the percentage of node population inside that grid. When each node is selecting its next destination (Section III-A, step 2), it first selects a grid following the probability μ_k, then randomly selects the next destination inside that grid, which is similar to [33] but without the Markovian process.

Before synthesizing traces, we run the closed loop pre-synthesis as described in Section III-D to obtain the appropriate interaction matrix Q. The maximum speeds are also adjusted during the closed loop cycles to approach the desired average speeds. The cycle period is set to 160 hours, which yields statistically significant results. We show the trends of convergence during the closed loop as well as the convergence results by the end of the pre-synthesis in Fig. 8. The trends of convergence are shown in Fig. 8(a)-(c) as the average difference between the actual and target mean (solid lines) and standard deviation (dashed lines) plotted against number of iterations. The convergence results are presented in Fig. 8(d)-(i) as the target mean $M_{i,j}$ and NSD $S_{i,j}$ versus the actual results $M'_{i,j}$ and $S'_{i,j}$, together with the solid lines whose slopes are the ratios between the actual and target mean or NSD of IRP distances $M^{\text{IRP}\prime}/M^{\text{IRP}}$ or $S^{\text{IRP}\prime}/S^{\text{IRP}}$. Ideally, in Fig. 8(a)-(c) all lines should converge to 0, and in Fig. 8(d)-(i) the solid lines should have a slope close to 1, which are the dashed lines, and the dots be closely distributed around the solid lines. Although the discrepancies suggest that there are limitations in our approach, the linearity shown in the convergence results indicates that the heterogeneity of inter-nodal distance in the input traces are sufficiently well captured and reproduced.

To further validate the N-Body model, we ran MANET simulations on the ns-2 simulator [38] using two representative routing protocols: the reactive AODV [39] and the proactive DSDV [40] on both the target and the synthesized traces. The contact ranges listed in Table II are heuristically determined according to the dimensions of the simulation area and the average node density. For comparison, we also show the results

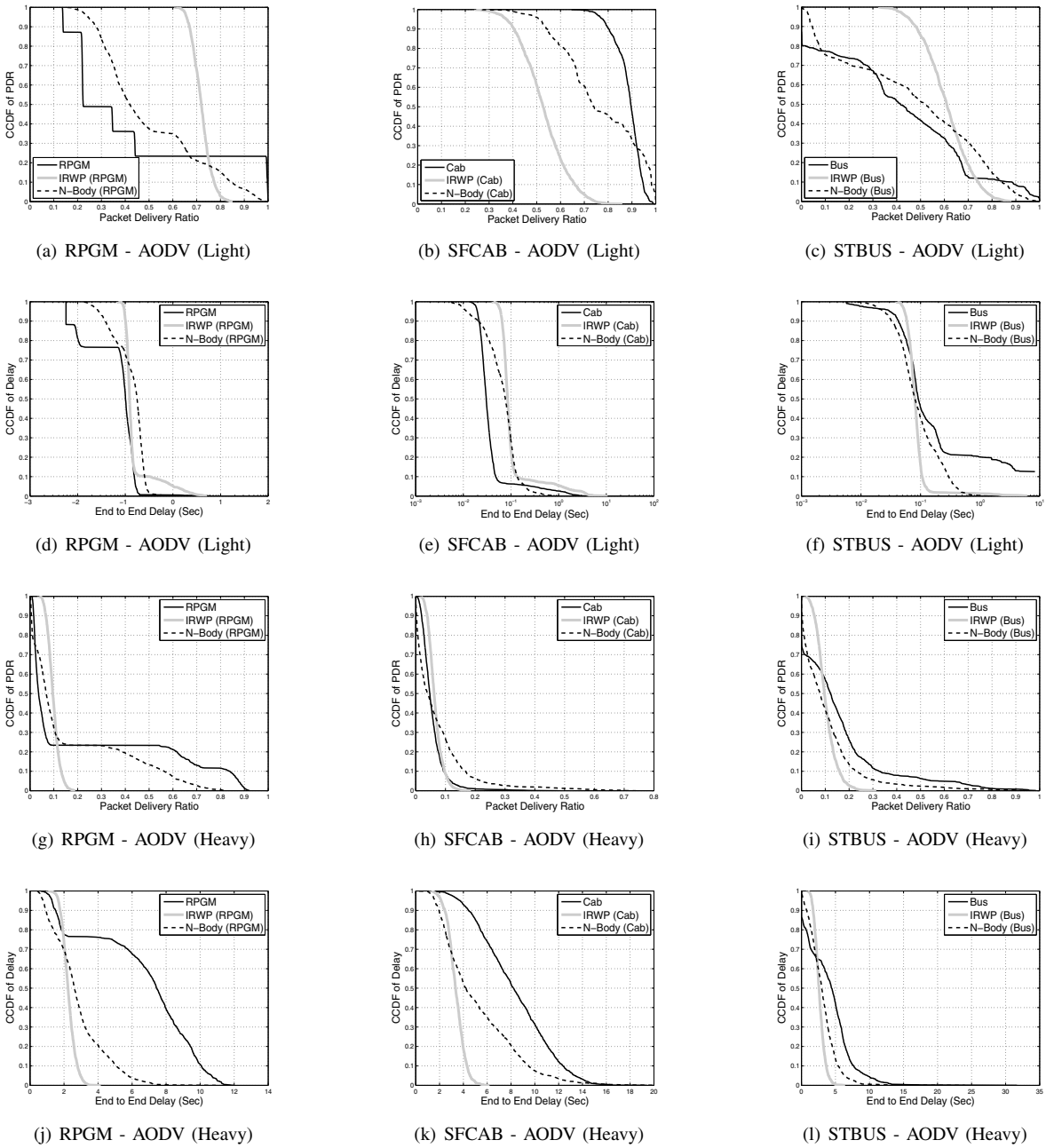

(a) RPGM - AODV (Light) (b) SFCAB - AODV (Light) (c) STBUS - AODV (Light)

(d) RPGM - AODV (Light) (e) SFCAB - AODV (Light) (f) STBUS - AODV (Light)

(g) RPGM - AODV (Heavy) (h) SFCAB - AODV (Heavy) (i) STBUS - AODV (Heavy)

(j) RPGM - AODV (Heavy) (k) SFCAB - AODV (Heavy) (l) STBUS - AODV (Heavy)

Fig. 9. AODV simulation results for light traffic (a)-(f) and heavy traffic (g)-(l): CCDF of pairwise packet delivery ratio (a)-(c),(g)-(i) and CCDF of pairwise delay (d)-(f),(j)-(l). Mobility models: (a)(d)(g)(j) RPGM, (b)(e)(h)(k) SFCAB, (c)(f)(i)(l) STBUS.

for *Improved Random Waypoint Models* (IRWP), which are RWP models that implement hotspots in the same way as in N-Body. The IRWP models use the exactly the same parameters as the corresponding N-Body models. Thus, they keep all the features of the corresponding N-Body models except the attraction and mutual forces.

Simulations are run with both light and heavy traffic. For light traffic packets are only sent between one pair of nodes. Packet size is set to 500 kB and 1 packet is generated each second. For heavy traffic simulation, all pairs of nodes simultaneously send packets at the same time and the packet rate is set to 1 packet per 3 seconds. In both simulations the average packet delivery ratio (PDR) and end-to-end delay are collected for each pair of nodes. The CCDF of the pairwise PDR and delay for all pairs of nodes are shown in Fig. 9. Due to space constraint, only the AODV results are shown. The DSDV results show trends that conform to that of AODV.

From Fig. 9, the curves of the N-Body models are always closer to those of real traces than the IRWP models, showing similar trends of heterogeneity. On the other hand, although the

IRWP models exhibit different results over different scenarios, all results approximately follow a normal distribution in their pairwise average values, which indicates a homogeneous inter-nodal relationship. Therefore, the N-Body model successfully captures the pairwise heterogeneity in the input traces, which mainly comes from the group-forming tendencies among nodes.

V. Conclusion and Future Work

In this paper we proposed the N-Body mobility model which is capable of synthesizing the group-forming tendency which can be observed from human movement traces. Compared to existing models, our model has the advantage of not requiring any knowledge of the social interaction in the target scenario, thus has wider scope of application. Our model is validated against the input traces both from real life and synthesized. Simulation results show that our model is capable of capturing and reproducing the heterogeneity in the input traces.

In the future work, a comprehensive analysis of the impact of such group-forming tendency upon network performance should be done, e.g., impact on protocol independent metrics like the link duration or inter-contact time. Methods of expanding the friendship and steadiness matrices from small populations to larger populations while maintaining a similar structure could also be explored. In addition, since heterogeneity may be also caused by geographical preference [20], [21], and such preference is common since real life human mobility are often non-stationary, incorporating such elements into N-Body model is also part of the future work.

References

[1] F. Bai, N. Sadagopan, and A. Helmy, "IMPORTANT: A framework to systematically analyze the impact of mobility on performance of routing protocols for ad hoc networks," in *Proc. IEEE INFOCOM'03*, San Francisco, CA, Apr. 2003.

[2] D. B. Johnson and D. A. Maltz, "Dynamic source routing in ad hoc wireless networks," in *Mobile Computing*, T. Imielinski and H. Korth, Eds. Norwell, MA, USA: Kluwer Academic Publishers, 1996, vol. 353, ch. 5, pp. 153–181.

[3] M. E. J. Newman and J. Park, "Why social networks are different from other types of networks," *Physical Review*, vol. 68, p. 036122, Sep. 2003.

[4] D. J. Watts and S. H. Strogatz, "Collective dynamics of 'small-world' networks," *Nature*, vol. 393, pp. 440–442, Jun. 1998.

[5] D. J. Watts, *Small Worlds: The Dynamics of Networks Between Order and Randomness*. Princeton, NJ: Princeton University Press, 1999.

[6] W.-J. Hsu and A. Helmy, "On nodal encounter patterns in wireless lan traces," in *Proc. IEEE WiOpt'06*, Boston, MA, Apr. 2006.

[7] P. Hui, J. Crowcroft, and E. Yoneki, "BUBBLE Rap: Social-based forwarding in delay tolerant networks," in *Proc. ACM MobiHoc'08*, Hong Kang SAR, China, May 2008.

[8] X. Hong, M. Gerla, G. Pei, and C.-C. Chiang, "A group mobility model for ad hoc wireless networks," in *Proc. ACM MSWiM'99*, Seattle, WA, Oct. 1999.

[9] B. Zhou, K. Xu, and M. Gerla, "Group and swarm mobility models for ad hoc network scenarios using virtual tracks," in *Proc. MILCOM'04*, Montery, CA, Nov. 2004.

[10] X. Lu, Y.-C. Chen, I. Leung, X. Zhang, and P. Liò, "A novel mobility model from a heterogeneous military manet trace," in *Proc. ADHOC-NOW'08*, Sophia-Antipolis, France, Sep. 2008.

[11] D. S. Tan, S. Zhou, J.-M. Ho, J. S. Mehta, and H. Tanabe, "Design and evaluation of an individually simulated mobility model in wireless ad hoc networks," in *Proc. CNDS'02*, San Antonio, TX, Jan. 2002.

[12] M. Rossi, L. Badia, N. Bui, and M. Zorzi, "On group mobility patterns and their exploitation to logically aggregate terminals in wireless networks," in *Proc. IEEE VTC'05*, Dallas, TX, Sep. 2005.

[13] S. A. Williams and D. Huang, "Group force mobility model and its obstacle avoidance capability," *Acta Astronautica*, vol. 65, Aug. 2009.

[14] K. Blakely and B. Lowekamp, "A structured group mobility model for the simulation of mobile ad hoc networks," in *Proc. MobiWac'04*, Philadelphia, PA, Oct. 2004.

[15] K. Herrmann, "Modeling the sociological aspects of mobility in ad hoc networks," in *Proc. ACM MSWiM'03*, San Diego, CA, Sep. 2003.

[16] M. Musolesi and C. Mascolo, "Designing mobility models based on social network theory," *Mobile Computing and Communications Review*, vol. 11, pp. 59–70, Jul. 2007.

[17] S. Gunasekaran and N. Nagarajan, "A new group mobility model for mobile adhoc network based on unified relationship matrix," *WSEAS Transactions on Communications*, vol. 7, pp. 58–67, Feb. 2008.

[18] P. Venkateswaran, R. Ghosh, A. Das, S. K. Sanyal, and R. Nandi, "An obstacle based realistic ad-hoc mobility model for social networks," *Journal of Networks*, vol. 1, no. 2, pp. 37–44, Jun. 2006.

[19] V. Borrel, F. Legendre, M. D. de Amorim, and S. Fdida, "SIMPS: Using sociology for personal mobility," *IEEE/ACM Transactions on Networking*, vol. 17, pp. 831–842, Jun. 2009.

[20] A. Mei and J. Stefa, "SWIM: A simple model to generate small mobile worlds," in *Proc. IEEE INFOCOM'09*, Rio de Janeiro, Brazil, Apr. 2009.

[21] K. Lee, S. Hong, S. J. Kim, I. Rhee, and S. Chong, "SLAW: A mobility model for human walks," in *Proc. IEEE INFOCOM'09*, Rio de Janeiro, Brazil, Apr. 2009.

[22] S. C. Nelson, A. F. Harris III, and R. Kravets, "Event-driven, role-based mobility in disaster recovery networks," in *Proc. CHANTS'07*, Montréal, Québec, Cancada, Sep. 2007.

[23] N. Aschenbruck, E. Gerhards-Padilla, M. Gerharz, M. Frank, and P. Martini, "Modeling mobility in disaster area scenarios," in *Proc. ACM MSWiM'07*, Chania, Crete Island, Greece, Oct. 2007.

[24] J. K. Frans Ekman, Ari Keränen and J. Ott, "Working day movement model," in *Proc. MobilityModels'08*, Hong Kong SAR, China, May 2008.

[25] V. Borrel, M. D. de Amorim, and S. Fdida, "A preferential attachment gathering mobility model," *IEEE Communications Letters*, vol. 9, no. 10, pp. 900–902, Oct. 2005.

[26] S. Lim, C. Yu, and C. R. Das, "Clustered mobility model for scale-free wireless networks," in *Proc. IEEE LCN'06*, Tampa, FL, Nov. 2006.

[27] C. W. Reynolds, "Flocks, herds, and schools: A distributed behavioral model," *Computer Graphics*, vol. 21, pp. 25–34, Jul. 1987.

[28] J. S. Bagla, "Cosmological n-body simulation: Techniques, scope and status," *Current Science*, vol. 88, pp. 1088–1100, Apr. 2005.

[29] J. G. Jetcheva, Y.-C. Hu, S. PalChaudhuri, A. K. Saha, and D. B. Johnson, "Design and evaluation of a metropolitan area multitier wireless ad hoc network architecture," in *the 5th IEEE Workshop on Mobile Computing Systems and Applications (WMCSA)*, Monterey, CA, Oct. 2003.

[30] M. Piorkowski, N. Sarafijanovoc-Djukic, and M. Grossglauser, "A parsimonious model of mobile partitioned networks with clustering," in *The First International Conference on COMmunication Systems and NETworkS*, Bangalore, India, Jan. 2009.

[31] C. Walsh, A. Doci, and T. Camp, "A call to arms: It's time for real mobility models," *Mobile Computing and Communications Review*, vol. 12, pp. 34–36, Jan. 2008.

[32] J. Yoon, B. D. Noble, M. Liu, and M. Kim, "Building realistic mobility models from coarse-grained traces," in *Proc. ACM MOBISYS'06*, Uppsala, Sweden, Jun. 2006.

[33] M. Kim, D. Kotz, and S. Kim, "Extract a mobility model from real user traces," in *Proc. IEEE INFOCOM'06*, Barcelona, Spain, Apr. 2006.

[34] M. Braun, *Differential Equations and Their Applications: An Introduction to Applied Mathematics*. New York, NY: Springer-Verlag, 1993.

[35] S. Scarle, "Highlighting a link between the Gay-Berne potential and the boid flocking model," *Simulation*, vol. 82, pp. 627–633, Oct. 2006.

[36] J. G. Gay and B. J. Berne, "Modification of the overlap potential to mimic a linear site-site potential," *The Journal of Chemical Physics*, vol. 74, no. 6, pp. 3316–3319, Mar. 1981.

[37] C. Bettstetter, H. Hartenstein, and X. Pérez-Costa, "Stochastic properties of the random waypoint mobility model," *Wireless Networks*, vol. 10, pp. 555–567, Sep. 2004.

[38] The network simulator - ns-2. http://www.isi.edu/nsnam/ns/.

[39] C. E. Perkins and E. M. Royer, "Ad-hoc on-demand distance vector routing," in *Proc. IEEE WMCSA'99*, New Orleans, LA, Feb. 1999.

[40] C. E. Perkins and P. Bhagwat, "Highly dynamic destination-sequenced distance-vector routing (dsdv) for mobile computers," *ACM SIGCOMM Computer Communication Review*, vol. 24, pp. 234–244, Oct. 1994.